

EFT observable stability under NLO corrections through interference revival

Céline Degrande^{1,*} and Matteo Maltoni^{1,†}

¹*Centre for Cosmology, Particle Physics and Phenomenology (CP3),
Université catholique de Louvain, 1348 Louvain-la-Neuve, Belgium*

We illustrate the importance of interference revival when higher order corrections are included, by presenting LO and NLO differential cross-sections and K -factors for three processes that are sensitive to the dimension-6 SMEFT operator O_W : Z -plus-two-jets (Zjj) production through Vector Boson Fusion (VBF), leptonic diboson WZ and $W\gamma$. We show how lifting the interference suppression at LO, through suitable variables and cuts, is necessary to get reliable predictions at NLO. We also show bounds on C_W obtained from these observables

Introduction Despite the achievements and success of accelerator physics in the past decades, no evidence for new resonances seems to be in sight in the near future; the presence of possible new heavy states can be investigated by searching for small anomalies in the interactions among the Standard Model (SM) particles. The Standard Model Effective Field Theory (SMEFT) provides a general tool to parametrise deviations from the SM, by adding to it complete sets of higher-dimensional operators O_i with coefficients C_i [1][2],

$$\mathcal{L}_{SMEFT} = \mathcal{L}_{SM} + \sum_i \frac{C_i}{\Lambda^2} O_i + \mathcal{O}(\Lambda^{-4}), \quad (1)$$

with Λ the new physics (NP) scale. The same expansion is observed in the differential cross-section for a generical measurable variable X ,

$$\frac{d\sigma}{dX} = \frac{d\sigma^{SM}}{dX} + \sum_i \frac{C_i}{\Lambda^2} \frac{d\sigma^{1/\Lambda^2}}{dX} + \mathcal{O}(\Lambda^{-4}). \quad (2)$$

It has been observed that the second term, being an interference between the SM amplitudes and the ones that are linear in C_i , can be suppressed for $2 \rightarrow 2$ processes [3] and in higher-multiplicity ones, resulting in the constraints coming from the term quadratic in C_i . Inspired by [4], in a previous work [5] we showed that efficient distributions can revive the sensitivity to the interference, providing constraints to the coefficient which are dominated by the leading ($\mathcal{O}(\Lambda^{-2})$) term. In this article, we show how the application of the same procedure is important to get stable predictions at Next-to-Leading Order in Quantum Chromodynamics (NLO QCD) for these operators; in particular, we focus on the O_W one, for which the large and negative K -factors computed at $\mathcal{O}(\Lambda^{-2})$ level [6] highlight the presence of a suppression at Leading Order (LO), lifted at NLO. The (differential) K -factor is defined as the ratio of the (differential) cross-sections at NLO and LO. Our analysis considers three processes that are sensitive to the effects of this operator, namely the fully leptonic electroweak (EW) Z -plus-two-jets production through Vector Boson Fusion (VBF), the fully leptonic $W^\pm Z$ diboson production, and the leptonic $W^\pm \gamma$; we show the predictions for some relevant distributions

in the SM and at linear and quadratic orders.

The approach described in this paper is more general and can be applied to any phase space cancellation of the interference, not only to the O_W case. In particular, if at least two operators affect one process, only one linear combination of them will impact the total interference cross-section, while all the others will be suppressed. Our approach is thus necessary to fully constrain those orthogonal directions of the parameter space, for which a cancellation occurs at linear level.

This method and the quantities it introduces can also be used together with machine-learning algorithms to develop suitable variables to restore the interference term or to compute asymmetries [7][8].

Framework The operator we consider in this work is a dimension-6 CP-even one and can be written as

$$O_W = \epsilon^{IJK} W_\mu^{I,\nu} W_\nu^{J,\rho} W_\rho^{K,\mu}, \quad (3)$$

where $W_\mu^{I,\nu}$ is the EW field strength. It directly contributes to diboson processes, triple gauge couplings and top EW production.

In our previous work [5], we introduced the integral of the absolute-valued interference differential cross-section,

$$\sigma^{|\text{int}|} = \int d\Phi \left| \frac{d\sigma^{1/\Lambda^2}}{d\Phi} \right|, \quad (4)$$

as an upper bound to the total effect of the interference, over the entire phase space Φ . A comparison between this and the actual cross-section gives an estimate of the suppression that affects the second one. This quantity, though, is not measurable, as it requires the knowledge of the initial states, neutrino momenta and jet flavors and helicities in the final state. The measurable absolute-valued cross-section is thus defined as

$$\sigma^{|\text{meas}|} = \int d\Phi_{\text{meas}} \left| \sum_{\{um\}} \frac{d\sigma^{1/\Lambda^2}}{d\Phi} \right|, \quad (5)$$

where the sum (integral) is performed over the set of discrete (continuous) unmeasurable quantities. This quantity is derived using only the information that is available in experiments, so it can be considered as an upper

bound for any asymmetry, built on kinematic variables by summing the absolute values of the bin contents of their distributions, with the aim to restore the interference. It can be estimated as

$$\sigma^{|\text{meas}|} = \lim_{N \rightarrow \infty} \sum_{i=1}^N w_i \times \text{sign} \left(\sum_{\{um\}} \text{ME}(\vec{p}_i, \{um\}) \right), \quad (6)$$

where ME is the interference part of the squared amplitude, w_i is the weight of the i^{th} event and \vec{p}_i are the momenta of its final states. This quantity is computationally expensive to obtain and it requires model assumptions, so our aim is to find easily-measurable kinematic variables that can approximate its value, in a general way that could be applied even outside the SMEFT framework or in regions where the EFT validity is questionable.

Our analysis is performed via MADGRAPH5_AMC@NLO v3.4.2 [9], which we fed the SMEFT@NLO [6] Universal FeynRules Output (UFO) [10], written from a FeynRules model [11] that contains most of the CP-even dimension-6 operators in the SMEFT; NLOCT is used to get the rational and ultraviolet counterterms [12]. The leptons and quarks, except the top one, are considered as massless. We use the NNPDF3.0 parton distribution function (PDF) set [13], with $\alpha_S(M_Z)=0.118$. In all the non-SM distributions and cross-sections presented in this paper, C_W/Λ^2 is set to 1 TeV⁻². For the calculations at NLO that are carried out at fixed order (FO), we set the renormalisation and factorisation scales $\mu_R = \mu_F = 1$ TeV; the events generated at NLO [14], on the other hand, are showered through PYTHIA8 [15] or HERWIG7 [16][17]. The sum of transverse energies divided by two $H_T/2$ is chosen as dynamical scale for the events. Jets are reconstructed using the anti- k_t algorithm [18][19], with a radius parameter $R = 0.4$.

Numerical and scale uncertainties are reported for each result [20]. Numerical errors are due to the limited number of events generated, while scale variations are computed by taking the envelope of nine scale combinations, in which $\mu_{R,F}$ are varied by factors 0.5 and 2.

For given distributions, we derive limits on the C_W value, by considering the deviations of each theory, namely $\sigma_{\text{best}}^{SM} + \frac{C_W}{\Lambda^2} \sigma^{1/\Lambda^2} \left(+ \frac{C_W^2}{\Lambda^4} \sigma^{1/\Lambda^4} \right)$ with the 2nd and 3rd terms at LO or NLO, from real data when possible, or from the best SM prediction $\sigma_{\text{best}}^{SM}$. In these bound computations, we associate in each bin relative errors to the LO interference and $\mathcal{O}(1/\Lambda^4)$ contributions equal to $|k_i - 1|$, with k_i the K -factor for the bin; for negative values or above 2, a 100% uncertainty is considered, since the scale variations cannot be considered a good estimate of the missing higher order corrections. For the SM and the terms at NLO, the numerical and scale uncertainties from our predictions are considered, being

the only available. As we can see for WZ production in the top plot of Fig. 6, NLO uncertainties from MADGRAPH5 do not include the N²LO results inside them. This suggests that all the error bars shown in the plots in this paper, even the NLO ones for the SM that enter the bound computations for C_W , might underestimate the true uncertainties. In case of lack of real data, we associate to the best SM prediction in the i^{th} bin a statistical uncertainty equal to $\sqrt{\sigma_{\text{best},i}^{SM}/\mathcal{L}_{LHC}}$, where the per bin cross-section is divided by the Large Hadron Collider (LHC) luminosity at Run II, $\mathcal{L}_{LHC}=137 \text{ fb}^{-1}$, plus a 10% systematic one; no correlation among different bins is assumed.

For each LO interference distributions, we also plot the relative cancellation

$$R_{w\pm} = \frac{\text{wgt} > 0 - \text{wgt} < 0}{\text{wgt} > 0 + \text{wgt} < 0}, \quad (7)$$

defined as the difference between the numbers of positive and negative weights in each bin, divided by their sum; the cancellation is larger where this ratio is closer to 0.

ELECTROWEAK Z + TWO JETS PRODUCTION THROUGH VECTOR BOSON FUSION

Computational details The EW Zjj production is characterised by the exchange of a weak vector boson in the t -channel. We consider the $Z \rightarrow \ell^+ \ell^-$ decay case, with $\ell = e, \mu$. Following ATLAS specifications [21], leptons are required to have transverse momentum $p_T > 25$ GeV and pseudo-rapidity $|\eta| < 2.4$; the total invariant mass of the leptons coming from the decay of the Z boson has to satisfy $81.2 < M_{\ell\ell} < 101.2$ GeV, and their total transverse momentum $p_T^{\ell\ell} > 20$ GeV.

We require a leading jet with $p_T > 85$ GeV and a sub-leading one with $p_T > 80$ GeV. The rapidity for each jet has to be $|y| < 4.4$ and a separation is required among them and the leptons, namely $\Delta R_{\ell j} > 0.4$ (we consider $\Delta R = \sqrt{\Delta\phi^2 + \Delta\eta^2}$ with $\Delta\phi, \Delta\eta$ the azimuthal and pseudorapidity distances).

The EW contribution to the process is characterised by a large invariant mass for the jets, $M_{jj} > 1$ TeV, and a large gap in rapidity among them, $|\Delta y_{jj}| > 2$. Furthermore, we impose the Z boson to be centrally produced relatively to the jets system, by asking $\xi_Z < 0.5$; the last quantity is defined as

$$\xi_Z = \frac{|y_{\ell\ell} - \frac{1}{2}(y_{j1} - y_{j2})|}{|\Delta y_{jj}|}, \quad (8)$$

with $y_{\ell\ell}, y_{j1}$ and y_{j2} the rapidities of the dilepton system, the leading and subleading jets.

Results An analysis by the ATLAS Collaboration [21][22], showed that the signed azimuthal angle difference between the two jets is particularly sensitive to the

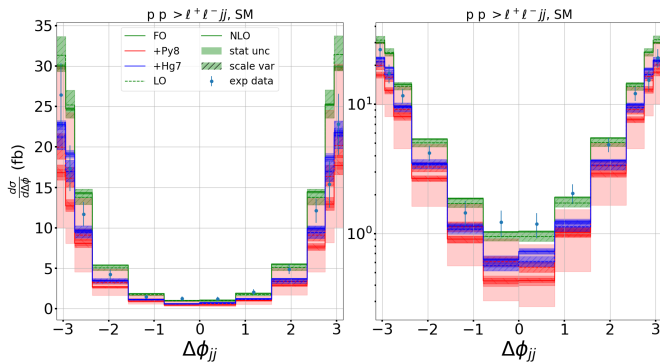


FIG. 1. LO and NLO SM differential distribution for the azimuthal distance between jets in EW Zjj , at FO and matched with PYTHIA8 and HERWIG7 showers. The two plots represent the same distributions, with linear (*left*) and logarithmic (*right*) scales on the vertical axis. Statistical and scale-variation uncertainties are shown, and the experimental data from [21] as well

O_W effects. This variable is defined as $\Delta\phi_{jj} = \phi_{j1} - \phi_{j2}$, where the jets are ordered in rapidity, such that $y_{j1} > y_{j2}$. The total LO and NLO cross-sections at FO for the SM, linear and quadratic contributions can be found in Table I, together with the relative K -factors. Our FO SM NLO fiducial total cross-section overestimates the ATLAS one by a factor ~ 1.5 ; it is known that predictions from different generators do not agree for the VBF processes [21][23][24] and that results heavily depend on the shower choice [25][26]. In Fig. 1, the differential distributions for $\Delta\phi_{jj}$ are shown for the LO and NLO SM matched with PYTHIA8, with HERWIG7 and at FO. PYTHIA8 usually applies the global recoil scheme, that is not suitable for VBF processes; a dipole recoil one should be employed instead [26], but this is possible in MADGRAPH5 only at LO, as the counterterms for the shower at NLO are derived assuming the global scheme. In terms of the total cross-section, the best agreement of SM predictions with ATLAS measurements is obtained when HERWIG7 is used, but at differential level, FO calculations seem to better agree in the central bins. Since the differential distribution is particularly important for O_W , we choose to use the FO generations in our analysis. However, the NLO + parton shower results for the interference between the SM and the dimension-6 operator show similar K -factors. In addition, choosing the generator and shower that more precisely reproduce the data with the SM results would fit away any room for new physics contributions.

The integral and the measurable absolute-valued cross-sections are shown in Table II for the interference contribution, together with the asymmetry measured by $\Delta\phi_{jj}$. These results come from LO event generation, with no parton shower applied. It can be seen that a suppression occurs for the interference, as its cross-section is much lower than σ^{int} and σ^{meas} , but that the di-jet azimuthal

difference can restore a large part of it.

The LO differential distributions for $\Delta\phi_{jj}$ are shown in Fig. 2, for both the SM and the linear term in C_W , with no parton shower. The positive- and negative-weighted contributions to the interference are also shown separately, confirming the ability of this observable to separate very well the opposite-sign components of the interference. The bins we use are $[0, \pi/4, \pi/2, 3\pi/4, 7\pi/8, 15\pi/16, \pi]$ and their symmetric around 0. The NLO predictions for the same distributions at FO are reported in Fig. 3, for the SM, $\mathcal{O}(\Lambda^{-2})$ and $\mathcal{O}(\Lambda^{-4})$ contributions. The K -factors are shown, for each bin, with the relative statistical and scale uncertainties, together with the cancellation level $R_{w\pm}$ in (7) for the LO interference. The differential K -factors are stable around 1 for this variable, as it happens for the total cross-section ones; indeed, the cancellation level is far from 0 in each bin.

We provide 68% and 95% Confidence Level (CL) bounds on C_W from this variable in Fig. 12. They are obtained by comparing the $\Delta\phi_{jj}$ distributions and the results in [21]. The NLO SM values we use come from the HERWIG7+VBFNLO prediction [27] in the ATLAS paper, while the linear and quadratic corrections are computed at FO. We use the correlation matrix from ATLAS for the statistical uncertainties, while the systematic and scale ones are added in quadrature on the diagonal.

It can be seen that the bounds from the interference only are comparable to the ones that include the quadratic term as well. Our bounds are of the same order of magnitude than the ones obtained by the ATLAS Collaboration.

FULLY LEPTONIC WZ PRODUCTION

Computational details We consider the $W^\pm Z$ diboson production, with leptonic decays $W^\pm \rightarrow \ell^\pm \nu_\ell^{(\pm)}$ and $Z \rightarrow \ell^+ \ell^-$, where $\ell = e, \mu$ and the sign refers to the electric charge. In case the three visible leptons are from the same family, the resonant shape algorithm described in [28] is used to assign each of them to their W or Z mother. The phase space is defined according to the criteria given by ATLAS in the same paper: the p_T of Z leptons ℓ_Z has to be above 15 GeV, while the W lepton ℓ_W one has to be higher than 20 GeV. For all the leptons, we require $|\eta| < 2.5$, and the invariant mass of the Z boson decay products, $M_{\ell_Z^+ \ell_Z^-}$, has to be higher than 81.2 and lower than 101.2 GeV. The angular distance between the two ℓ_Z must satisfy $\Delta R > 0.2$, while it has to be greater than 0.3 among ℓ_W and the two ℓ_Z . We furthermore demand the W transverse mass to be above 30 GeV; this variable is defined as $M_T^W = \sqrt{2p_T^\nu p_T^{\ell_W} (1 - \cos \Delta\phi_{\ell_W \nu})}$, with p_T^{ν, ℓ_W} the transverse momenta of the neutrino and W lepton, and $\Delta\phi_{\ell_W \nu}$ their azimuthal distance.

	SM	$\mathcal{O}(1/\Lambda^2)$	$\mathcal{O}(1/\Lambda^4)$
$pp \rightarrow \ell^+ \ell^- jj$ EW, $\ell = (e, \mu)$			
σ_{LO} (fb)	$49 \pm 0.06\%_{-6\%}^{+8\%}$	$-1.67 \pm 0.4\%_{-7\%}^{+6\%}$	$9.4 \pm 0.07\%_{-10\%}^{+11\%}$
σ_{NLO} (fb)	$52.2 \pm 0.19\%_{-1.1\%}^{+0.8\%}$	$-1.66 \pm 1.2\%_{-0.8\%}^{+0.4\%}$	$11.1 \pm 0.18\%_{-4\%}^{+3\%}$
K -factor	$1.07 \pm 0.19\%_{-7\%}^{+9\%}$	$0.99 \pm 1.2\%_{-8\%}^{+6\%}$	$1.18 \pm 0.17\%_{-14\%}^{+14\%}$
$pp \rightarrow \ell^\pm \nu^{(-)} \ell^+ \ell^-, \ell = (e, \mu)$			
σ_{LO} (fb)	$34.6 \pm 0.012\%_{-1.4\%}^{+1.2\%}$	$0.169 \pm 0.3\%_{-2\%}^{+1.8\%}$	$6.2 \pm 0.06\%_{-1.6\%}^{+2\%}$
σ_{NLO} (fb)	$50.5 \pm 0.02\%_{-1.4\%}^{+1.6\%}$	$-0.91 \pm 0.5\%_{-7\%}^{+5\%}$	$7.34 \pm 0.07\%_{-0.7\%}^{+0.8\%}$
σ_{N^2LO} (fb)	$62.8 \pm 0.3\%_{-1.3\%}^{+1.4\%}$	-	-
K -factor	$1.46 \pm 0.03\%_{-3\%}^{+3\%}$	$-5.4 \pm 0.6\%_{-9\%}^{+7\%}$	$1.18 \pm 0.09\%_{-3\%}^{+3\%}$
N^2LO / LO	$1.82 \pm 0.3\%_{-3\%}^{+3\%}$	-	-
$pp \rightarrow \ell^\pm \nu^{(-)} \gamma, \ell = (e, \mu, \tau)$			
σ_{LO} (fb)	$20.7 \pm 0.4\%_{-1.4\%}^{+1.4\%}$	$-0.67 \pm 9\%_{-9\%}^{+21\%}$	$110 \pm 0.5\%_{-4\%}^{+5\%}$
σ_{NLO} (fb)	$29.8 \pm 0.6\%_{-2\%}^{+3\%}$	$-3.4 \pm 9\%_{-11\%}^{+9\%}$	$121 \pm 0.7\%_{-1.2\%}^{+1.2\%}$
K -factor	$1.44 \pm 0.5\%_{-4\%}^{+4\%}$	$5.1 \pm 12\%_{-22\%}^{+29\%}$	$1.10 \pm 0.7\%_{-5\%}^{+6\%}$

TABLE I. Cross-section results in fb, for the SM, linear and quadratic contributions, for the fully leptonic EW Zjj , WZ and $W\gamma$ production; the total K -factors are also shown. C_W/Λ^2 is set to 1 TeV $^{-2}$. For each result, the first uncertainty source is statistical, while the second ones come from scale variation. For the K -factors, the statistical uncertainty is propagated in quadrature from the cross-section ones, while for the scale variation, the total envelope is considered. These results were obtained through FO computations for the first two processes, while the last one is matched to parton shower. The WZ results are averaged over four decay channels

The main issue in this process is represented by the presence of a neutrino in the final state: since its momentum cannot be measured, we follow the standard strategy of reconstructing it by imposing the $M_{\ell_W \nu}$ invariant mass to be equal to the W pole mass M_W [29][30]. From this requirement, up to two possible solutions are obtained, and there is no way to affirm which of them is correct. Previous studies [31] verified that choosing the one which is smaller in absolute value is more efficient than a completely random extraction, so this is the strategy we adopt. In reality, being the W boson virtual, its mass is not equal to M_W ; even if this criterion provides a good approximation of the true value, there are events in which no real solutions come from this requirement. The neutrino is thus reconstructed by discarding their imaginary part.

To be able to compare with the experimental results in [28], all the cross-sections and distributions for this process are averaged over the four different $e^\pm \nu_e e^+ e^-$, $e^\pm \nu_e \mu^+ \mu^-$, $\mu^\pm \nu_\mu \mu^+ \mu^-$, $\mu^\pm \nu_\mu e^+ e^-$ channels; uncertainties are propagated in the average assuming total correlation among them.

Results The LO and NLO total cross-sections at FO are shown in Table I, along with the total K -factors and their uncertainties. For the SM, the N^2LO cross-section from MATRIX [32–39] is also reported, together with the N^2LO/LO ratio: these results are compatible with [40][41] and the ATLAS ones. The integral and measurable absolute-valued cross-sections are shown in Table II.

By comparing the actual interference cross-section with these values, it can be noticed that a large suppression occurs. This is partially lifted when the events in which the negatively-charged Z lepton ℓ_Z^- has helicity $h=+1$ or -1 are considered separately: as it can be seen in the Table, the ratios of the measurable over the integral cross-sections increase when this distinction is applied. Even if Z leptons helicity values are not experimentally accessible, better predictions can come from variables that are sensible to them.

In [30] and [42], it is shown that the interference between the O_W operator and the SM in WZ production is proportional to

$$\phi_{WZ} = \cos(2\phi_W) + \cos(2\phi_Z), \quad (9)$$

where ϕ_V , $V = W, Z$, is the azimuthal angle between the plane containing the V boson and the beam axis, and the plane where its decay products lie, in lab frame. The direction of the latter is defined as the vectorial product of the positive- and negative-helicity lepton three-momenta; since the Z boson couplings to left- and right-handed leptons are similar, this can be determined only up to an overall sign. This introduces an ambiguity on $\phi_Z \longleftrightarrow \phi_Z - \pi$, which however does not affect the value of ϕ_{WZ} , as it is a function of $\cos(2\phi_Z)$. For what concerns the W boson, the lepton helicities are constrained by the left-handed nature of the interaction, but another ambiguity is introduced by the presence of a neutrino, whose momentum can only be reconstructed. This partially washes away the $2\phi_W$ modulations in the variable above.

	(fb)	% of σ^{int}	% of σ^{meas}
$pp \rightarrow \ell^+ \ell^- jj$ EW, $\ell = (e, \mu)$			
σ^{int}	$13.27 \pm 0.3\%$	100	-
σ^{meas}	$12.81 \pm 0.3\%$	97	100
$\Delta\phi_{jj}$	$11.42 \pm 0.4\%$	89	86
$\sigma_{LO}^{1/\Lambda^2}$	$-1.71 \pm 2\%$	13	13
$pp \rightarrow \ell^\pm \ell^\mp \ell^\pm \ell^\mp, \ell = (e, \mu)$			
σ^{int}	$4.93 \pm 0.4\%$	100	-
σ^{meas}	$2.04 \pm 1.0\%$	41	100
$p_T^Z \times \phi_{WZ}$	$1.31 \pm 1.5\%$	27	64
ϕ_{WZ}	$0.79 \pm 3\%$	16	39
M_T^{WZ}	$0.66 \pm 3\%$	13	32
$\cos\theta_{\ell^- Z}^*$	$0.20 \pm 10\%$	4	10
$\sigma_{LO}^{1/\Lambda^2}$	$0.20 \pm 10\%$	4	10
$h(\ell_Z^-) = -1, h(\ell_Z^+) = +1$			
σ^{int}	$2.773 \pm 0.5\%$	100	-
σ^{meas}	$1.738 \pm 0.9\%$	63	100
M_T^{WZ}	$0.38 \pm 4\%$	14	21
$\sigma_{LO}^{1/\Lambda^2}$	$0.108 \pm 14\%$	4	6
$h(\ell_Z^-) = +1, h(\ell_Z^+) = -1$			
σ^{int}	$2.135 \pm 0.6\%$	100	-
σ^{meas}	$1.067 \pm 1.1\%$	50	100
M_T^{WZ}	$0.289 \pm 4\%$	14	27
$\sigma_{LO}^{1/\Lambda^2}$	$0.087 \pm 14\%$	4	8
$p_T^Z > 50 \text{ GeV AND } \phi_{WZ} > -0.5$			
σ^{int}	$2.260 \pm 0.7\%$	100	-
σ^{meas}	$0.873 \pm 1.7\%$	39	100
M_T^{WZ}	$0.660 \pm 2\%$	29	76
$\sigma_{LO}^{1/\Lambda^2}$	$0.660 \pm 2\%$	29	76
$p_T^Z < 40 \text{ GeV OR } \phi_{WZ} < -1$			
σ^{int}	$1.810 \pm 0.5\%$	100	-
σ^{meas}	$0.870 \pm 1.1\%$	48	100
M_T^{WZ}	$0.480 \pm 2\%$	27	55
$\sigma_{LO}^{1/\Lambda^2}$	$-0.480 \pm 2\%$	27	55
$pp \rightarrow \ell^\pm \ell^\mp \nu \gamma, \ell = (e, \mu, \tau)$			
σ^{int}	$31.44 \pm 0.3\%$	100	-
σ^{meas}	$12.50 \pm 0.9\%$	40	100
ϕ_W	$9.90 \pm 1.1\%$	31	79
$p_T^Z \times \phi_W $	$9.90 \pm 1.1\%$	31	79
$p_T^Z \times \phi_f $	$1.44 \pm 7\%$	5	12
$\sigma_{LO}^{1/\Lambda^2}$	$-1.44 \pm 7\%$	5	12

TABLE II. LO $\mathcal{O}(1/\Lambda^2)$ integral and measurable absolute-valued cross-sections for Zjj , WZ and $W\gamma$, in fb. For the second process, the cases in which the Z leptons helicities are separated are also shown, together with the regions in (10). The absolute asymmetries for some relevant variables are reported: they are the sum of the absolute values of the bin contents. These results come from event generation at LO, without parton shower. The statistical uncertainties are shown: they are computed separately on the positive- and negative-weighted events through gaussian approximation of a Poisson distribution, then propagated in quadrature

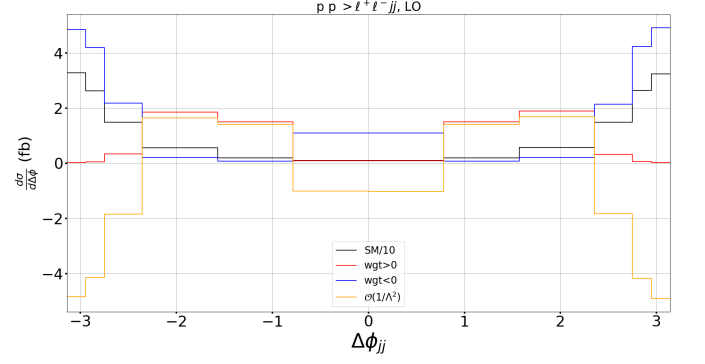


FIG. 2. Differential cross-section for the signed azimuthal distance between jets in Zjj , at LO without parton shower. The black line reproduces the SM distribution, divided by 10, while the red (blue) one the positive- (negative-) weighted contribution to the interference term. The orange line is the difference of the last two, namely the interference differential cross-section. The uncertainties are not shown

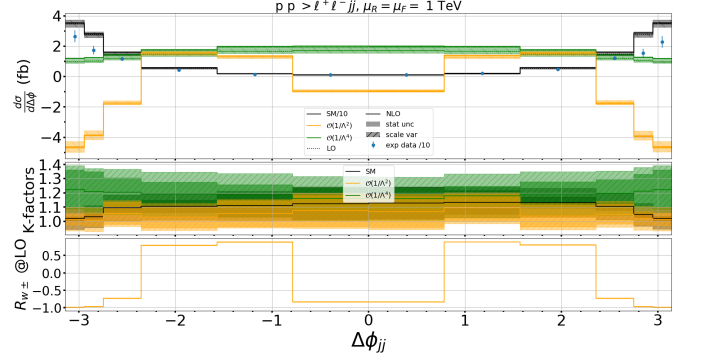


FIG. 3. FO NLO (continuous) and LO (dotted) differential cross-sections for $\Delta\phi_{jj}$ in Zjj , with the K -factors and cancellation level (7) for LO interference in each bin. The black (orange, green) line refers to the SM, divided by 10 (linear, quadratic terms); the statistical uncertainties and scale variations are also shown in the first two panels, while the last one only contains the statistical ones. Experimental data from [21] is represented by the blue dots with error bars, divided by 10

The $\mathcal{O}(1/\Lambda^2)$ double differential distribution for ϕ_{WZ} and the transverse momentum of the reconstructed Z boson, p_T^Z , shows similar behaviours when the separation between the events with $h(\ell_Z^-) = -1$ and $h(\ell_Z^-) = +1$ is applied, while the same does not hold for many other observables. This can be seen in Fig. 4 for the interference at LO. By cutting the phase-space in areas in which this double distribution is mainly positive or negative, we can obtain stable and reasonable K -factors for the variables computed over this process. In particular, the overall positive and negative regions are respectively delimited by

$$p_T^Z > 50 \text{ GeV AND } \phi_{WZ} > -0.5, \quad (10a)$$

$$p_T^Z < 40 \text{ GeV OR } \phi_{WZ} < -1. \quad (10b)$$

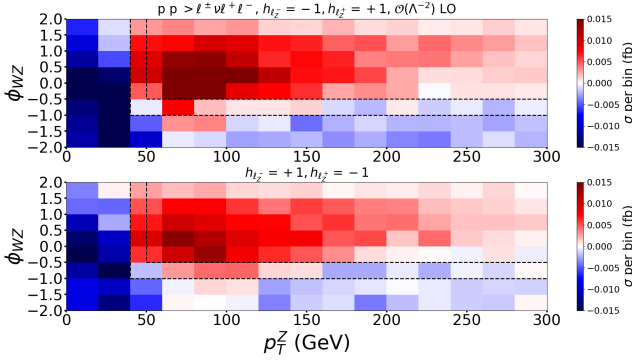


FIG. 4. WZ interference cross-section per bin at LO without parton shower, as a function of p_T^Z and ϕ_{WZ} , in the two cases in which the Z leptons have helicities ± 1 and ∓ 1 . Red (blue) areas mark where the cross-section is positive (negative), as the positive- (negative-) weighted contribution dominates there. The black dashed lines separate the phase space areas in (10)

In the phase-space portion in between these two regions, the LO double distribution changes its sign, yielding unstable and large K -factors.

The NLO and LO distributions of ϕ_{WZ} , for the SM, interference and quadratic correction, are shown in Fig. 5, with the relative differential K -factors and cancellation level. In the top plot, that considers the whole phase space, it can be seen that the $\mathcal{O}(1/\Lambda^2)$ K -factors present jumps or become large when the cancellation is almost complete. When the distributions are computed in the phase space regions defined by the cuts (10), the K -factors are more reasonable: the cancellation $R_{w\pm}$ is always positive for the first cut and always negative for the second, as the opposite-sign weights at LO are partially separated. We use bins of 0.4 from -2 to 2.

For the SMEFT interpretation, the WZ transverse mass has been considered in previous studies [22][28]; this variable is defined as

$$M_T^{WZ} = \sqrt{\left(\sum_{\ell} p_T^{\ell} + p_T^{\nu}\right)^2 - \left(\sum_{\ell} \vec{p}_T^{\ell} + \vec{p}_T^{\nu}\right)^2}, \quad (11)$$

where the sums include the charged leptons. This distribution is useful to probe those SMEFT operators whose effects increase with the center-of-mass energy \sqrt{s} . The LO and NLO plots for this observable are presented in Fig. 6, for the SM, linear and quadratic terms, together with $R_{w\pm}$ and the differential K -factors. It can be seen how these are more regular when the cuts (10) over ϕ_{WZ} and p_T^Z are applied, showing that less suppression is present in these phase space regions. For the whole phase space case, SM N²LO predictions from MATRIX are also plotted, together with the N²LO/LO differential ratio and data from [28]. The bins are delimited at [0, 140, 180, 250, 450, 600, 13000] GeV.

Another previous work [43], about SMEFT corrections

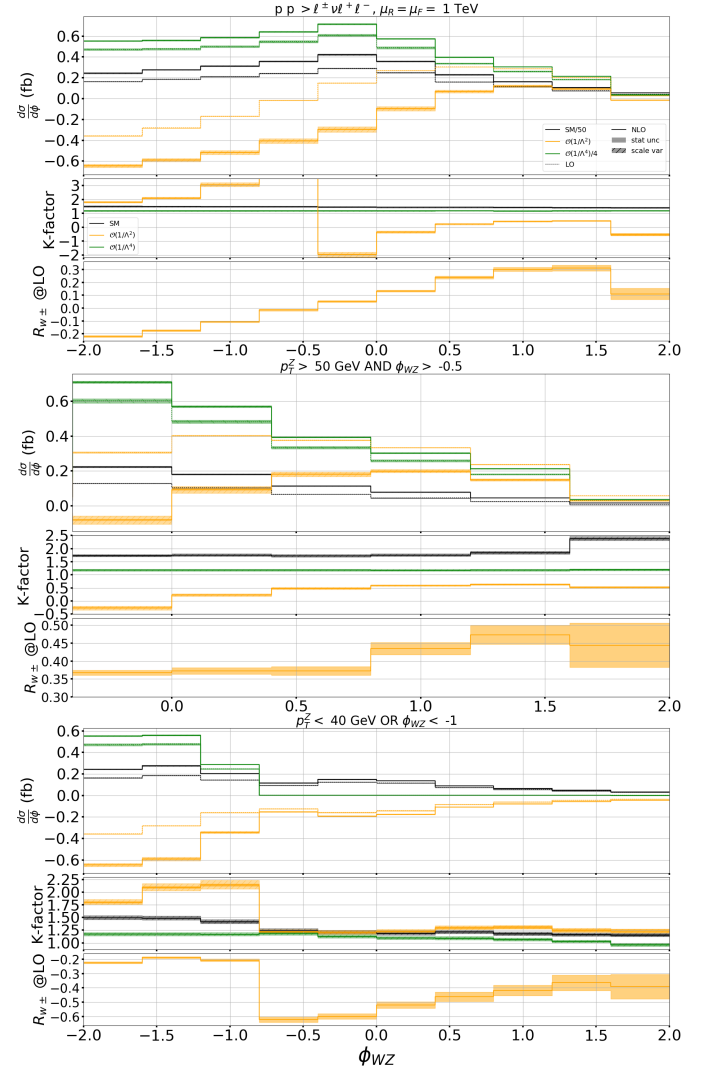


FIG. 5. LO and NLO differential cross-section distributions, for ϕ_{WZ} , over all the phase space (*top*) and when specific cuts on p_T^Z and ϕ_{WZ} are applied (*center* and *bottom*). The black (orange, green) line represents the SM, divided by 50 (interference, quadratic correction divided by 4). The K -factors are also shown, together with their statistical and scale uncertainties. For each case, the relative cancellation for LO interference is plotted. Note the different variable range in the central plot, due to the cuts

to WZ production, suggests other angular variables that are sensitive to new physics effects. In particular, we focus on $\cos\theta_{\ell_Z^*}^{*}$, the cosine of the angle between the negatively-charged Z lepton three-momentum, in the Z boson rest frame, and the direction of flight of the boson, seen in the center-of-mass (com) frame; this coordinate system is defined in [44]. The com reference system reconstruction is affected by the neutrino momentum ignorance. The LO SM distribution for this variable is sensitive to the ℓ_Z helicity configurations, as it can be seen in Fig. 7: the two plots have different trends, with

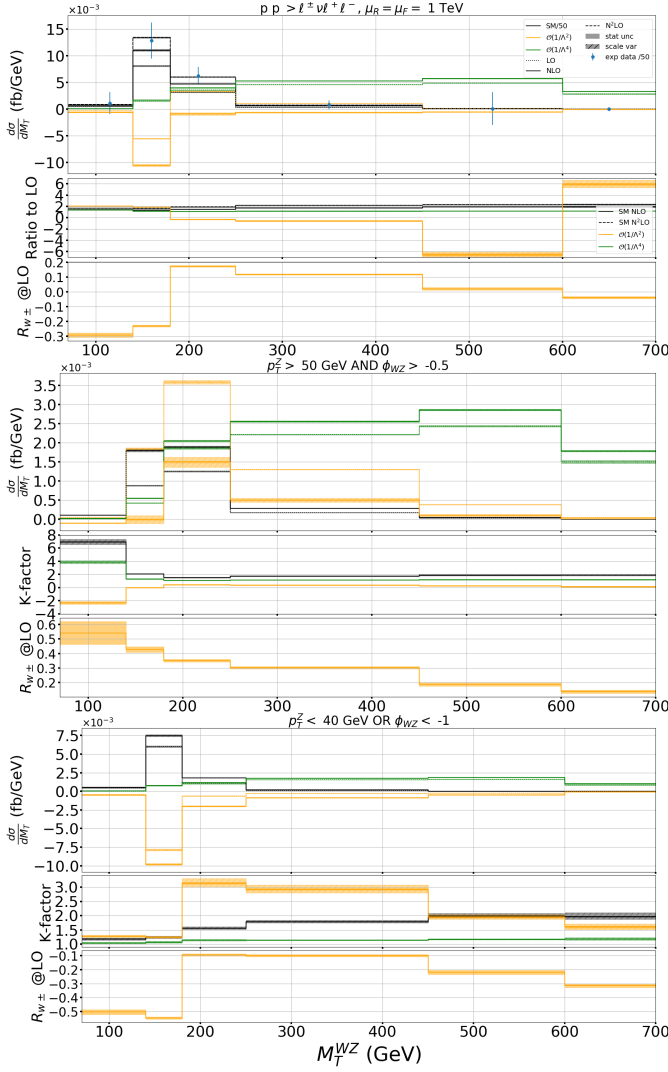


FIG. 6. FO LO and NLO differential cross-section distributions, for the transverse mass of the WZ system, over all the phase space (*top*) and when cuts on p_T^Z and ϕ_{WZ} are applied (*center* and *bottom*). The black (orange, green) line represents the SM, divided by 50 (interference, NP squared). The K -factors are also shown, together with the relative cancellation for LO interference. In the first plot, we also report N^2 LO results for the SM at FO and the experimental data from [28], divided by 50. The last bin contains the overflow, up to 13 TeV

more events close to a variable value of -1 or 1 in the two cases. This dependency, though, is not evident in the $\mathcal{O}(1/\Lambda^2)$ term. The K -factors for this observable are shown in Fig. 8: while they are, at interference level, all negative when considering the whole phase space, they improve when the cuts (10) are applied, as the LO and NLO distributions have same sign in the two regions. We use bins of 0.2 from -1 to 1.

The C_W bounds we obtained from M_T^{WZ} are shown in Fig. 12, on the whole phase space and in the two regions defined in (10). In the first case, the limits come from

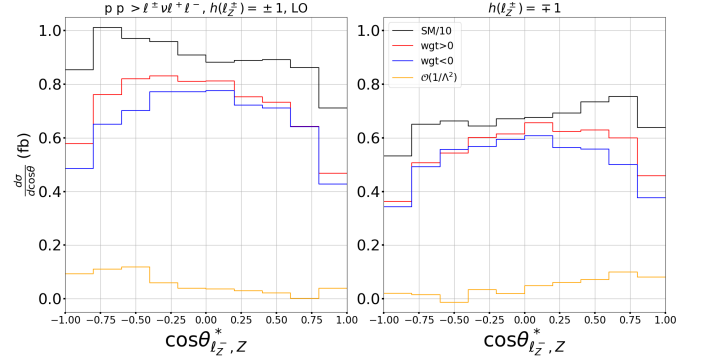


FIG. 7. LO SM and interference distributions (without parton shower) for $\cos \theta_{\ell_Z}^*$, splitted according to the Z lepton helicity. The positive- and negative-weighted contributions to the linear cross-section term are shown in red and blue. The uncertainties are not reported

the comparison with results in [28], using the correlation matrix given there for statistical uncertainties, while the scale variation ones are summed in quadrature on the diagonal. In the special regions, due to the lack of real data, we confront predictions with our SM NLO one. It can be seen that the limits from LO interference improve when the p_T^Z, ϕ_W cuts are applied, and that in region (10a) they are more stringent at LO than NLO due to the K -factors being smaller than one. The region (10b) provides constraints that are quite stronger than the full phase space ones.

LEPTONIC W + PHOTON PRODUCTION

Computational details We present some predictions for the $W^\pm \gamma$ production, with the W boson decaying as $W^\pm \rightarrow \ell^\pm \nu_\ell^{(-)}$. All three lepton families are considered: $\ell = e, \mu, \tau$, with no decay for the τ . The phase space is delimited as for the EFT analysis in [45] by the CMS Collaboration: a minimum p_T of 80 GeV and a maximum $|\eta|$ of 2.5 are required for the lepton, while for the neutrino we demand $p_T > 40$ GeV. For the photon, requirements include $p_T > 150$ GeV, $|\eta| < 2.5$, $\Delta R_{\ell\gamma} > 0.7$. No jet with $p_T > 30$ GeV and $|\eta| < 2.5$ is allowed. Scale variation uncertainties for the interference were obtained by generating samples with both μ_R and μ_F divided or multiplied by 2, and then considering the envelope.

Results The total cross-sections, at LO and NLO, and the K -factors are summarised in Table I, together with the statistical and scale uncertainties. They come from NLO event generation matched with PYTHIA8. Table II reports the measurable and integral absolute-valued cross-sections; the comparison with the interference total one reveals a large suppression at LO. The large difference among the interference cross-section re-

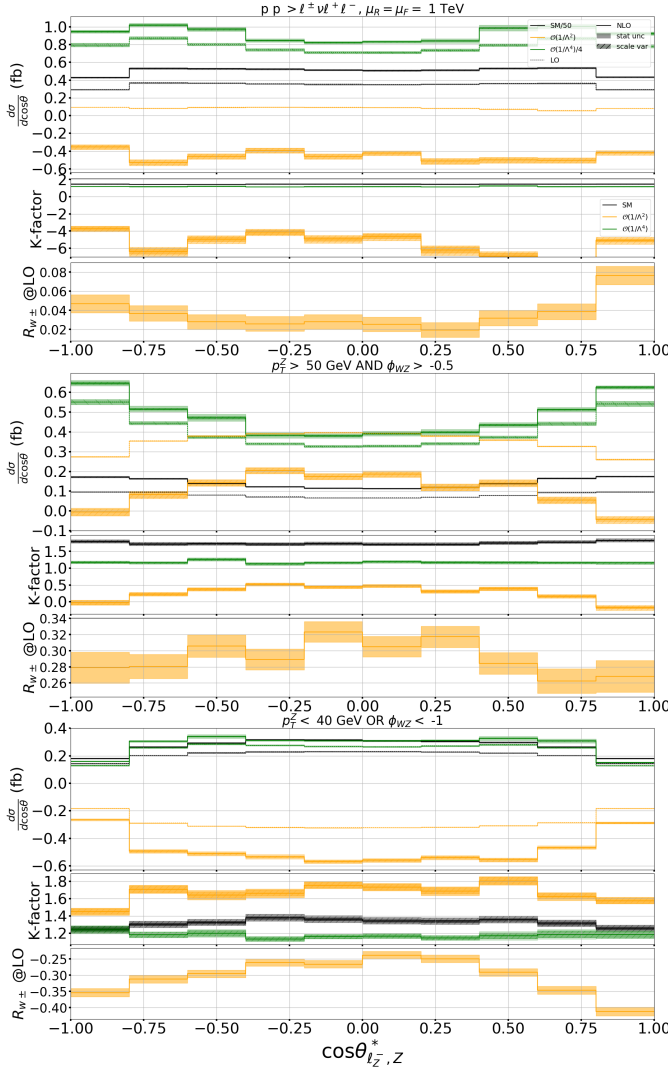


FIG. 8. FO LO and NLO differential cross-section distributions, for $\cos\theta_{\ell_Z}^*$, over all the phase space (*top*) and when phase space cuts are applied (*center* and *bottom*). The black (orange, green) line represents the SM, divided by 50 (interference, quadratic term divided by 4). The K -factors are also shown, together with the relative cancellation for LO interference

sults in the two Tables is a parton shower effect, as many events gain a jet after it and need to be discarded for the above-mentioned requirements. As in the Zjj case, an observable is able to considerably lift the interference cancellation: this is the azimuthal angle ϕ_W between the plane with the W boson and the beam axis, and the plane where the decay products lie, in lab frame; it is analogous to the ones defined in (9). The neutrino momentum reconstruction, carried on as for WZ , introduces an ambiguity in this observable value; this does not prevent from observing the interference effects, since they are proportional to $\cos(2\phi_W)$ [30]. The LO, NLO and K -factor distributions for this variable are shown

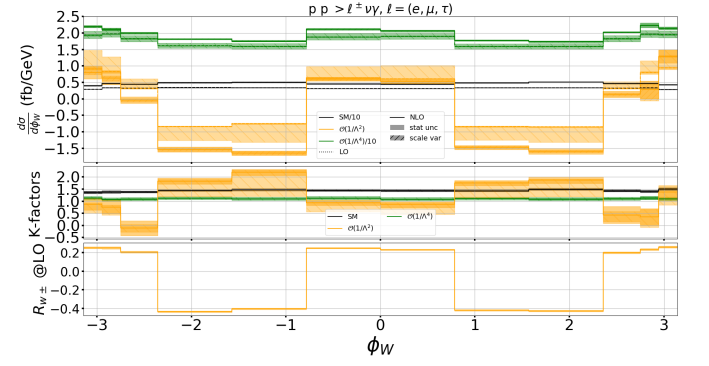


FIG. 9. LO and NLO differential cross-sections and K -factors for ϕ_W , at SM, interference and quadratic orders. The statistical and scale uncertainties are reported for each result. The relative cancellation between positive- and negative-weighted events is plotted for the interference at LO, with statistical error bars

in Fig. 9 for the SM, interference and NP squared, together with the cancellation level. The bins we use are $[0, \pi/4, \pi/2, 3\pi/4, 7\pi/8, 15\pi/16, \pi]$ and their symmetric around 0.

In the CMS paper, the angle ϕ is introduced in the com frame as the ℓ^\pm azimuthal angle, with the \hat{z} axis along the W^\pm three-momentum and $\hat{y} = \hat{r} \times \hat{z}$, where \hat{r} denotes the Lorentz-boost direction from the lab frame. Given the ambiguity in ϕ , due to the neutrino reconstruction, the angle ϕ_f is used, with $\phi_f = \phi$ if $|\phi| < \pi/2$, or $\phi_f = \pi - \phi$ if $\phi > \pi/2$ and $\phi_f = -(\pi + \phi)$ if $\phi < -\pi/2$. The EFT analysis is carried on through the double distribution of p_T^γ and $|\phi_f|$, with three bins of $\pi/6$ from 0 to $\pi/2$ for the angle, and $[150, 200, 300, 500, 800, 1500]$ GeV for the photon transverse momentum.

The LO and NLO distributions of p_T^γ , split according to the $|\phi_f|$ interval and with their K -factors and $R_{w\pm}$, are shown in Fig. 10, for the SM, interference and quadratic correction.

It can be seen from Table II that the $p_T^\gamma \times |\phi_f|$ distribution at LO is as suppressed as the total interference cross-section. As a comparison, we show the LO and NLO double distribution for $p_T^\gamma \times |\phi_W|$, which is sensible to a larger fraction of σ^{meas} , in Fig. 11; we use the same binning for the transverse momentum, and $[0, \pi/4, 3\pi/4, \pi]$ for the absolute value of the angle. The K -factors and their uncertainties are more stable and reasonable in these plots, as the LO and NLO interference distributions have the same sign in the three regions delimited by $|\phi_W|$, positive in the external ones and negative in the central.

The bounds on C_W from the two double distributions are shown in Fig. 12. The limits from the $p_T^\gamma \times |\phi_W|$ variable are obtained out of comparison with the SM NLO distribution we generated, while the bounds for the $p_T^\gamma \times |\phi_f|$ double distribution come from confrontation with the data in [45]. Since no correlation matrix is available, we assume no correlation among different bins for

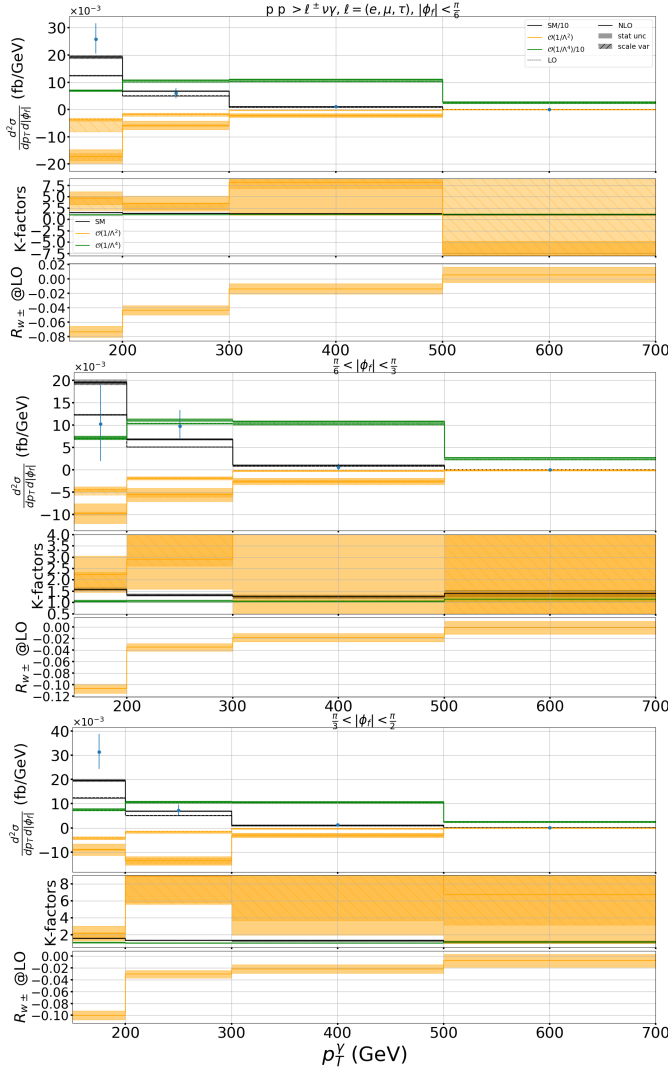


FIG. 10. LO and NLO double differential distribution of $p_T^\gamma \times |\phi_f|$. The black (orange, green) line shows the SM divided by 10 (interference, NP squared divided by 10). The blue dots with error bars represent the experimental data from [45], divided by 10. The K -factors and the $\mathcal{O}(1/\Lambda^2)$ cancellation are also reported

the ϕ_W case; for ϕ_f , the matrix given in the CMS paper is used for statistical uncertainties, while scale variation ones are added in quadrature on the diagonal. The bounds we obtain from $p_T^\gamma \times |\phi_W|$ are better than the ones from $p_T^\gamma \times |\phi_f|$ already at LO for the interference.

CONCLUSIONS

In this paper, we showed some results for three process that are affected by the O_W operator, for which the linear correction to the SM is suppressed: EW Zjj VBF, WZ and $W\gamma$ production. We reported differential distributions for relevant variables, at LO and NLO, for the

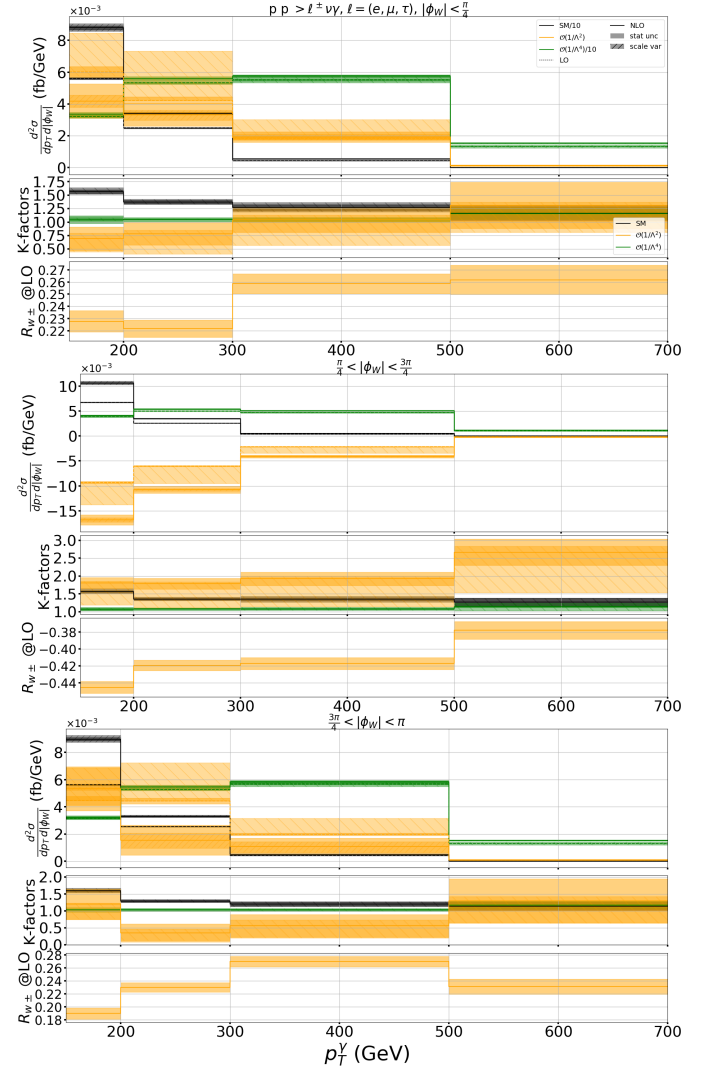


FIG. 11. LO and NLO double differential distribution of $p_T^\gamma \times |\phi_W|$. The black (orange, green) line shows the SM divided by 10 (interference, NP squared divided by 10). The K -factors and the $\mathcal{O}(1/\Lambda^2)$ cancellation are also reported

SM, the linear and the quadratic corrections. We showed how the choice of these variables is important to improve the new physics predictions when the interference is suppressed, and how the K -factors display a perturbative expansion under better control and, therefore, better uncertainties when the positive- and negative-weighted components of the interference at LO are separated with suitable phase space cuts. We also reported bounds on the operator coefficient from the comparison among our predictions and real data, showing how some differential distributions can provide limits that, at linear level, are comparable with the ones from the quadratic order, which does not experience the same cancellation. These variables are fully generic, since they only depend on the kinematics, and do not rely on model assumptions as much as the matrix element method does. The corre-

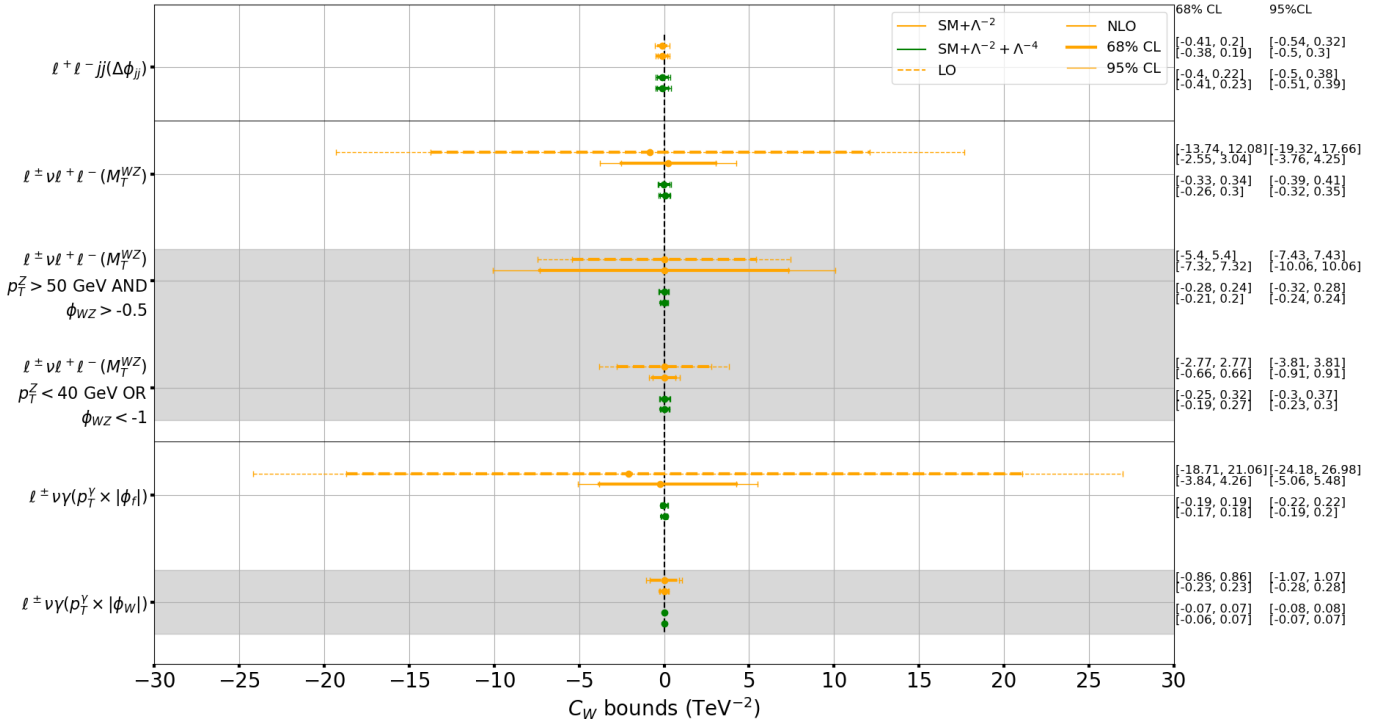


FIG. 12. 68% and 95% CL LO (dashed) and NLO (continuous) bounds on the C_W coefficient, with and without the inclusion of the quadratic term, coming from Zjj VBF, $W^\pm Z$ and $W^\pm \gamma$. For the second process, we show the limits over the whole phase space and in the two regions (10); for the last one, limits from two double distributions are reported. The variables we use are noted next to the process definitions. The bounds in the gray area come from comparison with the best SM distribution we obtain, while the others with real data. The numerical values are reported on the right

sponding predictions can also be updated at any order, due to this model independence. The techniques introduced in this paper can be used in conjunction with machine learning to get better predictions for the interference among the SM and SMEFT operators. We showed that, in general, a low cancellation over the phase space is needed to obtain meaningful predictions for the interference with respect to higher order terms. Although we focused here on QCD corrections, we expect this conclusion to be valid for EW ones as well. In particular, the very good revival obtained in VBF through the $\Delta\phi_{jj}$ distribution suggests that, even if the EW corrections are expected to be large for the interference, they should not yield K -factors too far from unity. The same statement cannot be affirmed with the same confidence in the diboson cases, as the unmeasurable cancellation is larger. However, $W\gamma$ displays a strong constraining power, similar to VBF, when interference-reviving distributions are used.

Acknowledgments Computational resources have been provided by the Consortium des Équipements de Calcul Intensif (CÉCI), funded by the Fonds de la Recherche Scientifique de Belgique (F.R.S.-FNRS) under Grant No. 2.5020.11 and by the Walloon Region. MM is a Research Fellow of the F.R.S.-FNRS, through the grant

Aspirant. We are thankful to F. Maltoni, E. Vryonidou, G. Durieux, K. Mimasu, A. Pilkington, N. Clarke Hall and A. Gilbert for discussion and very useful suggestions during this work.

* celine.degrande@uclouvain.be

† matteo.maltoni@uclouvain.be

- [1] B. Grzadkowski, M. Iskrzynski, M. Misiak, and J. Rosiek, “Dimension-Six Terms in the Standard Model Lagrangian,” *JHEP* **10**, 085 (2010), [arXiv:1008.4884 \[hep-ph\]](https://arxiv.org/abs/1008.4884).
- [2] W. Buchmuller and D. Wyler, “Effective Lagrangian Analysis of New Interactions and Flavor Conservation,” *Nucl. Phys. B* **268**, 621–653 (1986).
- [3] A. Azatov, R. Contino, C.S. Machado, and F. Riva, “Helicity selection rules and noninterference for BSM amplitudes,” *Phys. Rev. D* **95**, 065014 (2017), [arXiv:1607.05236 \[hep-ph\]](https://arxiv.org/abs/1607.05236).
- [4] L. Dixon and Y. Shadmi, “Testing gluon self-interactions in three-jet events at hadron colliders,” *Nuclear Physics B* **423**, 3–32 (1994).
- [5] C. Degrande and M. Maltoni, “Reviving the interference: Framework and proof-of-principle for the anomalous gluon self-interaction in the SMEFT,” *Physical Review D* **103** (2021), [10.1103/physrevd.103.095009](https://arxiv.org/abs/10.1103/physrevd.103.095009).

- [6] C. Degrande, G. Durieux, F. Maltoni, K. Mimasu, E. Vryonidou, and C. Zhang, “Automated one-loop computations in the standard model effective field theory,” *Physical Review D* **103** (2021), 10.1103/physrevd.103.096024.
- [7] A. Bhardwaj, C. Englert, R. Hankache, and A.D. Pilkington, “Machine-enhanced CP-asymmetries in the Higgs sector,” *Physics Letters B* **832** (2022), 10.1016/j.physletb.2022.137246.
- [8] N. Clarke Hall, I. Criddle, A. Crossland, C. Englert, P. Forbes, R. Hankache, and A.D. Pilkington, “Machine-enhanced CP-asymmetries in the electroweak sector,” (2023), [arXiv:2209.05143 \[hep-ph\]](#).
- [9] J. Alwall, R. Frederix, S. Frixione, V. Hirschi, F. Maltoni, O. Mattelaer, H.-S. Shao, T. Stelzer, P. Torrielli, and M. Zaro, “The automated computation of tree-level and next-to-leading order differential cross sections, and their matching to parton shower simulations,” *Journal of High Energy Physics* **2014** (2014), 10.1007/jhep07(2014)079.
- [10] C. Degrande, C. Duhr, B. Fuks, D. Grellscheid, O. Mattelaer, and T. Reiter, “UFO - The Universal Feyn-Rules Output,” *Comput. Phys. Commun.* **183**, 1201–1214 (2012), [arXiv:1108.2040 \[hep-ph\]](#).
- [11] A. Alloul, N.D. Christensen, C. Degrande, C. Duhr, and B. Fuks, “FeynRules 2.0 - A complete toolbox for tree-level phenomenology,” *Comput. Phys. Commun.* **185**, 2250–2300 (2014), [arXiv:1310.1921 \[hep-ph\]](#).
- [12] C. Degrande, “Automatic evaluation of UV and R2 terms for beyond the Standard Model Lagrangians: a proof-of-principle,” *Computer Physics Communications* **197**, 239–262 (2015), [arXiv:1406.3030 \[hep-ph\]](#).
- [13] R.D. Ball, V. Bertone, S. Carrazza, C.S. Deans, L. Del Debbio, S. Forte, A. Guffanti, N.P. Hartland, J.I. Latorre, and et al., “Parton distributions for the LHC run II,” *Journal of High Energy Physics* **2015** (2015), 10.1007/jhep04(2015)040.
- [14] S. Frixione and B.R. Webber, “Matching NLO QCD computations and parton shower simulations,” *Journal of High Energy Physics* **2002**, 029–029 (2002).
- [15] T. Sjöstrand, S. Ask, J.R. Christiansen, R. Corke, N. Desai, P. Ilten, S. Mrenna, S. Prestel, C.O. Rasmussen, and P.Z. Skands, “An introduction to PYTHIA 8.2,” *Computer Physics Communications* **191**, 159–177 (2015).
- [16] M. Bähr, S. Gieseke, M.A. Gigg, D. Grellscheid, K. Hamilton, O. Latunde-Dada, S. Plätzer, P. Richardson, M.H. Seymour, A. Sherstnev, and B.R. Webber, “Herwig++ physics and manual,” *The European Physical Journal C* **58**, 639–707 (2008).
- [17] J. Bellm, S. Gieseke, D. Grellscheid, S. Plätzer, M. Rauch, C. Reuschle, P. Richardson, P. Schichtel, M.H. Seymour, A. Siódmok, A. Wilcock, N. Fischer, M.A. Harrendorf, G. Nail, A. Papaefstathiou, and D. Rauch, “Herwig 7.0/Herwig++ 3.0 release note,” *The European Physical Journal C* **76** (2016), 10.1140/epjc/s10052-016-4018-8.
- [18] M. Cacciari, G.P. Salam, and G. Soyez, “The anti-kt jet clustering algorithm,” *Journal of High Energy Physics* **2008**, 063–063 (2008).
- [19] M. Cacciari, G.P. Salam, and G. Soyez, “FastJet user manual (for version 3.0.2),” *The European Physical Journal C* **72** (2012), 10.1140/epjc/s10052-012-1896-2.
- [20] R. Frederix, S. Frixione, V. Hirschi, F. Maltoni, R. Pittau, and P. Torrielli, “Four-lepton production at hadron colliders: aMC@NLO predictions with theoretical uncertainties,” *Journal of High Energy Physics* **2012** (2012), 10.1007/jhep02(2012)099.
- [21] ATLAS Collaboration, “Differential cross-section measurements for the electroweak production of dijets in association with a Z boson in proton–proton collisions at ATLAS,” *The European Physical Journal C* **81** (2021), 10.1140/epjc/s10052-020-08734-w.
- [22] ATLAS Collaboration, “Combined effective field theory interpretation of differential cross-sections measurements of WW, WZ, 4l, and Z-plus-two-jets production using ATLAS data,” *ATL-PHYS-PUB-2021-022* (2021).
- [23] ATLAS Collaboration, “Observation of Electroweak Production of a Same-Sign W boson pair in association with two jets in pp collisions at $\sqrt{s} = 13$ TeV with the ATLAS detector,” *Physical Review Letters* **123** (2019), 10.1103/physrevlett.123.161801.
- [24] ATLAS Collaboration, “Modelling of the vector boson scattering process $pp \rightarrow W^\pm W^\pm jj$ in Monte Carlo generators in ATLAS,” *ATL-PHYS-PUB-2019-004* (2019).
- [25] S. Höche, S. Mrenna, S. Payne, C.T. Preuss, and P. Skands, “A Study of QCD Radiation in VBF Higgs Production with Vincia and Pythia,” (2021), [arXiv:2106.10987 \[hep-ph\]](#).
- [26] B. Jäger, A. Karlberg, S. Plätzer, J. Scheller, and M. Zaro, “Parton-shower effects in Higgs production via vector-boson fusion,” *The European Physical Journal C* **80** (2020), 10.1140/epjc/s10052-020-8326-7.
- [27] J. Baglio, J. Bellm, G. Bozzi, M. Brieg, F. Campanario, C. Englert, B. Feigl, J. Frank, T. Figy, F. Geyer, C. Hackstein, V. Hankele, B. Jäger, M. Kerner, M. Kubocz, L.D. Ninh, C. Oleari, S. Palmer, S. Plätzer, M. Rauch, R. Roth, H. Rzehak, F. Schissler, O. Schlimpert, M. Spannowsky, M. Worek, and D. Zeppenfeld, “VBFNLO: A parton level Monte Carlo for processes with electroweak bosons – Manual for Version 2.7.0,” (2011), 10.48550/arXiv.1107.4038, [arXiv:1107.4038](#).
- [28] M. Aaboud, G. Aad, B. Abbott, O. Abdinov, B. Abeoos, D.K. Abhayasinghe, S.H. Abidi, O.S. AbouZeid, N.L. Abraham, and et al., “Measurement of $W^\pm Z$ production cross sections and gauge boson polarisation in pp collisions at $\sqrt{s} = 13$ TeV with the ATLAS detector,” *The European Physical Journal C* **79** (2019), 10.1140/epjc/s10052-019-7027-6.
- [29] G. Panico, F. Riva, and A. Wulzer, “Diboson interference resurrection,” *Physics Letters B* **776**, 473–480 (2018).
- [30] A. Azatov, D. Barducci, and E. Venturini, “Precision diboson measurements at hadron colliders,” *Journal of High Energy Physics* **2019** (2019), 10.1007/jhep04(2019)075.
- [31] R. Rahaman and R.K. Singh, “Unravelling the anomalous gauge boson couplings in ZW^\pm production at the LHC and the role of spin-1 polarizations,” *Journal of High Energy Physics* **2020** (2020), 10.48550/arXiv.1911.03111.
- [32] M. Grazzini, S. Kallweit, and M. Wiesemann, “Fully differential NNLO computations with MATRIX,” (2017), [arXiv:1711.06631 \[hep-ph\]](#).
- [33] T. Gehrmann, A. von Manteuffel, and L. Tancredi, “The two-loop helicity amplitudes for $q\bar{q}' \rightarrow V_1 V_2 \rightarrow 4$ leptons,” *JHEP* **09**, 128 (2015), [arXiv:1503.04812 \[hep-ph\]](#).
- [34] A. Denner, S. Dittmaier, and L. Hofer, “Collier: a fortran-based Complex One-Loop Library in Extended Regularizations,” *Comput. Phys. Commun.* **212**, 220–238 (2017), [arXiv:1604.06792 \[hep-ph\]](#).

- [35] F. Cascioli, P. Maierhofer, and S. Pozzorini, “Scattering Amplitudes with Open Loops,” *Phys. Rev. Lett.* **108**, 111601 (2012), [arXiv:1111.5206 \[hep-ph\]](#).
- [36] F. Buccioni, J.-N. Lang, J.M. Lindert, P. Maierhofer, S. Pozzorini, H. Zhang, and M.F. Zoller, “OpenLoops 2,” *Eur. Phys. J. C* **79**, 866 (2019), [arXiv:1907.13071 \[hep-ph\]](#).
- [37] F. Buccioni, S. Pozzorini, and M. Zoller, “On-the-fly reduction of open loops,” *Eur. Phys. J. C* **78**, 70 (2018), [arXiv:1710.11452 \[hep-ph\]](#).
- [38] S. Catani, L. Cieri, D. de Florian, G. Ferrera, and M. Grazzini, “Vector boson production at hadron colliders: hard-collinear coefficients at the NNLO,” *Eur. Phys. J. C* **72**, 2195 (2012), [arXiv:1209.0158 \[hep-ph\]](#).
- [39] S. Catani and M. Grazzini, “An NNLO subtraction formalism in hadron collisions and its application to Higgs boson production at the LHC,” *Phys. Rev. Lett.* **98**, 222002 (2007), [arXiv:hep-ph/0703012 \[hep-ph\]](#).
- [40] M. Grazzini, S. Kallweit, D. Rathlev, and M. Wiesemann, “ $W^\pm Z$ production at the LHC: fiducial cross sections and distributions in NNLO QCD,” (2017), [arXiv:1703.09065 \[hep-ph\]](#).
- [41] M. Grazzini, S. Kallweit, D. Rathlev, and M. Wiesemann, “ $W^\pm Z$ production at hadron colliders in NNLO QCD,” *Phys. Lett. B* **761**, 179–183 (2016), [arXiv:1604.08576 \[hep-ph\]](#).
- [42] A. Azatov, J. Elias-Miró, Y. Reyimuaji, and E. Venturini, “Novel measurements of anomalous triple gauge couplings for the LHC,” *Journal of High Energy Physics* **2017** (2017), [10.1007/jhep10\(2017\)027](#).
- [43] J. Baglio, S. Dawson, and S. Homiller, “QCD corrections in Standard Model EFT fits to WZ and WW production,” *Physical Review D* **100** (2019), [10.1103/physrevd.100.113010](#).
- [44] Z. Bern, G. Diana, L.J. Dixon, F.F. Cordero, D. Forde, T. Gleisberg, S. Höche, H. Ita, D.A. Kosower, D. Maître, and et al., “Left-handed W bosons at the LHC,” *Physical Review D* **84** (2011), [10.1103/physrevd.84.034008](#).
- [45] CMS Collaboration, “ $W^\pm \gamma$ differential cross sections and effective field theory constraints at $\sqrt{s} = 13$ TeV,” *Phys. Rev. D* **105** (2022), <https://doi.org/10.1103/PhysRevD.105.052003>.